In-plane anisotropic effect of magnetoelectric coupled PMN-PT/FePt multiferroic heterostructure: Static and microwave properties

Jose M. Vargas and Javier Gómez

Citation: APL Materials **2**, 106105 (2014); doi: 10.1063/1.4900815
View online: http://dx.doi.org/10.1063/1.4900815
View Table of Contents: http://scitation.aip.org/content/aip/journal/aplmater/2/10?ver=pdfcov
Published by the AIP Publishing

APL MATERIALS **2**, 106105 (2014)

In-plane anisotropic effect of magnetoelectric coupled PMN-PT/FePt multiferroic heterostructure: Static and microwave properties

Jose M. Vargas[a] and Javier Gómez[b]
Centro Atómico Bariloche (CNEA), Instituto Balseiro (U. N. Cuyo) and Conicet, 8400 San Carlos de Bariloche, Río Negro, Argentina

(Received 25 August 2014; accepted 20 October 2014; published online 31 October 2014)

The effects of the electric and magnetic field variation on multiferroic heterostructure were studied in this work. Thin films of polycrystalline $Fe_{50}Pt_{50}$ (FePt) were grown by *dc*-sputtering on top of the commercial slabs of lead magnesium niobate-lead titanate (PMN-PT). The sample was a (011)-cut single crystal and had one side polished. In this condition, the PMN-PT/FePt operates in the L-T (longitudinal magnetized-transverse polarized) mode. A FePt thin film of 20 nm was used in this study to avoid the characteristic broad microwave absorption line associated with these films above thicknesses of 40 nm. For the in-plane easy magnetization axis (01-1), a microwave magnetoelectric (ME) coupling of 28 Oe cm kV^{-1} was estimated, whereas a value of 42 Oe cm kV^{-1} was obtained through the hard magnetization axis (100). Insight into the effects of the in-plane strain anisotropy on the ME coupling is obtained from the *dc*-magnetization loops. It was observed that the trend was opposite along the easy and hard magnetic directions. In particular, along the easy-magnetic axis (01-1), a square and narrow loop with a factor of M_r/M_S of 0.96 was measured at 10 kV/cm. Along the hard-magnetic axis, a factor of 0.16 at 10 kV/cm was obtained. Using electric tuning via microwave absorption at X-band (9.78 GHz), we observe completely different trends along the easy and hard magnetic directions; Multiple absorption lines along the latter axis compared to a single and narrower absorption line along the former. In spite of its intrinsic complexity, we propose a model which gives good agreement both for static and microwave properties. These observations are of fundamental interest for future ME microwave components, such as filters, phase-shifters, and resonators. [http://dx.doi.org/10.1063/1.4900815]

The next generation of dual electric (E)- and magnetic (H)- tunable *RF* and microwave components, such as filters, attenuators, phase-shifters, and resonators, requires an improvement in the quality factor of the magnetoelectric coupling.[1,2] With this aim, the engineering of materials that simultaneously combines a large intrinsic piezoelectric and magnetostriction response becomes very attractive. However, it is also important to obtain a narrow ferromagnetic absorption line.[3,4] Since the ferromagnetic frequency becomes a key metric in the design of microwave devices, the ferromagnetic resonance and linewidth have a critical role in determining the frequency bandwidth of these components.[5] In fact, due to the intrinsic incompatibility between strong ferroelectric and ferromagnetic orders, only few readily available single phase materials possess both characteristics, at room temperature. Thus, in the recent years it has been observed that layered composites combining ferrites with ferroelectric materials can be an alternative path to reach these demands.[6] Lead magnesium niobate-lead titanate (PMN-PT) is one of such material, displaying a giant strain

[a]Electronic mail: jmvargas@ieee.org
[b]Electronic mail: gomezj@cab.cnea.gov.ar

hysteresis with tunable remanent properties.[7,8] In particular, (011)-cut ferroelectric PMN-PT single crystals possess superior anisotropic in-plane piezoelectric coefficients with a negative d_{31} of -890 pC N^{-1} and a positive d_{32} of 290 pC N^{-1}.[3,7]

Alloys of Fe with Pt are also of significant technological interest because of their unique magnetic properties. Thin films of these alloys grow in a metastable chemically disordered fcc phase (generally called A_1 phase) which has a similar value of the saturation magnetization of ordered $L1_0$ phase but a much smaller anisotropy and coercive field.[9] It is these characteristics of the A_1 FePt which render them desirable for RF/microwave devices. The thickness and temperature dependence of the dynamic magnetic behavior in A_1 FePt films were studied and reported by our research group elsewhere.[10] Briefly, annealing as-grown disordered FePt films at temperatures above 200 °C promotes the transformation to the $L1_0$ phase. This phase has large anisotropy which causes drastic changes in the microwave ferromagnetic resonance (FMR) spectrum of the resonance lines associated to the A_1 phase. For temperatures above 200 °C, the FMR absorption linewidth gradually broadens and the line intensity degrades significantly if the annealing temperature exceeded 300 °C. In fact, the line intensity decreases by more than 3 orders of magnitude for annealing temperatures up to 400 °C and is almost completely lost for annealing temperatures above 500 °C.[9] Furthermore, our research group reported[11] the microwave broadband magnetic properties of thin films of FePt alloy (in the chemically disordered fcc phase) with thicknesses ranging from 9 nm to 94 nm, where it was possible to observe a narrow ferromagnetic linewidth resonance in the frequency range up to 100 GHz. This was due to the fact that the magnetic domain structure in the form of stripes disappears at thicknesses below 40 nm.[11] A high saturation magnetostriction coefficient of FePt (~34 ppm)[12] compares well with values ~0.5 reported for FeGaB films (~70 ppm)[13] which are well established magnetostrictive alloys that exhibit both large magnetostriction and low magnetic anisotropy at room temperature.[14] The strong piezoelectricity of PMN-PT and magnetostriction of FePt alloys make the composite an optimal combination for magnetoelectric coupling mediated by stress. Since the magnetoelectric coupling is mediated by stress in PMN-PT alloys, it is therefore instructive to study this effect along the two main easy and hard magnetization axes to enable future optimization of RF/microwave devices.

To understand the intrinsic microwave properties and magnetoelectric tunable response of (011)-cut PMN-PT/Fe-Pt, we have investigated the E-field and H-field variation of the magnetization through static magnetization loops and dynamic absorption microwave response at X-band (9.78 GHz). The measurements were done in-plane, along the easy (01-1) and hard (100) magnetization axes. In this work, a 20 nm thin film of FePt alloy (using a target with nominal 50/50 atomic composition, in the chemically disordered fcc phase) was grown by dc-sputtering on top of the one side polished (011)-cut PMN-PT commercial slab (with pre-prepared electrodes). Following the same protocol mentioned elsewhere,[10] the chamber was pumped down to a base pressure of 10^{-7} Torr and the film was sputtered using 3 mTorr of Ar pressure, a power of 20 W, and a target-substrate distance of 10 cm. With these parameters, we obtained a sputtering rate of 0.15 nm/s.

The PMN-PT crystal was purchased from MTI Corporation, had a nominal thickness 0.05 cm, and was not poled. To improve the coupling between layers, the electrodes were grown by first sputtering a thin layer (5 nm) of titanium on each side of the PMN-PT slab, followed by 70 nm of silver layer electrodes on each side (see supplementary material for sample details and microstructure, Figure S1[15]). The microstructure and surface magnetic domain structure of FePt films were studied with a Veeco Dimension 3100 AFM/magnetic force microscopy (MFM) with Nanoscope IV electronics. To characterize the structural crystallinity of the (011)-cut PMN-PT slab and FePt films, X-ray diffraction measurements (XRD) in $\theta - 2\theta$ scans were carried out. Ferroelectricity was characterized using a commercial ferroelectric tester, Premier II. To reach high E-fields, we used a High-Voltage (10 kV) unit with a HVDM test fixture. A magneto-optic Kerr magnetometer was used for static magnetization loops acquisition. FMR spectra have been acquired at room temperature using a commercial Bruker ESP300 spectrometer at frequency ν = 9.78 GHz (X band). The samples were placed in the center of the resonant cavity, where the derivative of the absorbed power was measured using a standard field modulation and lock-in detection technique with amplitude of 20 Oe. The sample could be rotated inside the resonator in order to measure the resonance field for different orientations.

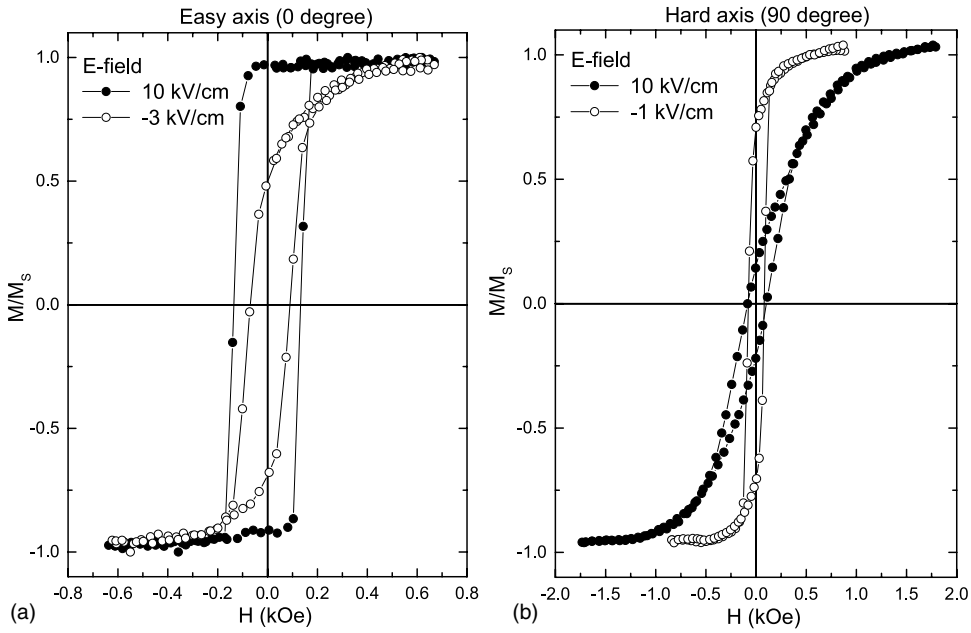

FIG. 1. E-field magnetization loops measured along the (a) easy magnetization axis (0°), at 10 kV/cm and −3 kV/cm; and (b) hard magnetization axis (90°), at 10 kV/cm and −1 kV/cm.

FePt films with thicknesses below 30 nm show the presence of a very limited number of magnetic domains (see supplementary material for details of magnetic images, Figure S2[15]). The XRD data confirm that the rhombohedral phase is the main crystal structure of the (011)-cut single crystal PMN-PT ferroelectric slab. The XRD pattern measured in a control sample of relatively thick FePt film (100 nm) confirms the chemically disordered A_1 fcc phase with [111] texture (see supplementary material for details of X-ray patterns and structural information, Figures S3 and S4, respectively[15]).

In-plane magnetization loops of the composite measured at room temperature shown in Fig. 1 confirm the strong anisotropic magnetoelectric (ME) coupling effect. Typical E-field magnetization loops measured along the easy (0°) and hard (90°) magnetization axes show the basic difference between both orientations. The E-field magnetization loops shown were measured using the following protocol: with the sample positioned in each respective orientation, the sample is initially poled at the maximum E-field value of −10 kV/cm. Next, the E-field is switched to the opposite value of +10 kV/cm and the magnetization loops were measured at each E-field value going forward from +10 kV/cm to −10 kV/cm. The field is then scanned from −10 kV/cm to +10 kV/cm. The squareness aspect ratio is defined as the remanent magnetization normalized by the saturation magnetization (M_r/M_S). The difference between the easy and hard magnetization axes is striking. For the case of the easy axis (Fig. 1(a), E-field of 10 kV/cm and −3 kV/cm), a squarer shape aspect of the magnetization loops can be noticed. On the other hand, magnetization loops measured along the hard magnetization axis look flat and linear (Fig. 1(b), E-field of 10 kV/cm and −1 kV/cm). In both cases, these loops reveal a sharp and asymmetric change of the squareness factor ratio (Fig. 2), which in case of the easy axis, range from 0.96 at 10 kV/cm to 0.5 at −3 kV/cm. When the E-field is swept between ±10 kV/cm, there is a change of a factor of 50%. Indeed, the variation of the squareness factor against E-field exhibited a butterfly curve, where the maximum squareness factor is reached at ±10 kV/cm and the minimum factor is obtained at ±2 kV/cm (Fig. 2(a)). Similarly, the variation of the squareness factor against E-field along the hard magnetization axis also exhibits a butterfly curve. However, compared with the former case, the hard axis orientation has an opposite trend which can be noticed: a minimum value at ±10 kV/cm ($M_r/M_S = 0.16$) and a maximum value close to ±2 kV/cm ($M_r/M_S = 0.63$). In both cases, easy and hard magnetic axis orientations, Fig. 2 summarizes the variation of the squareness factor against E-field. The insets on the top of each

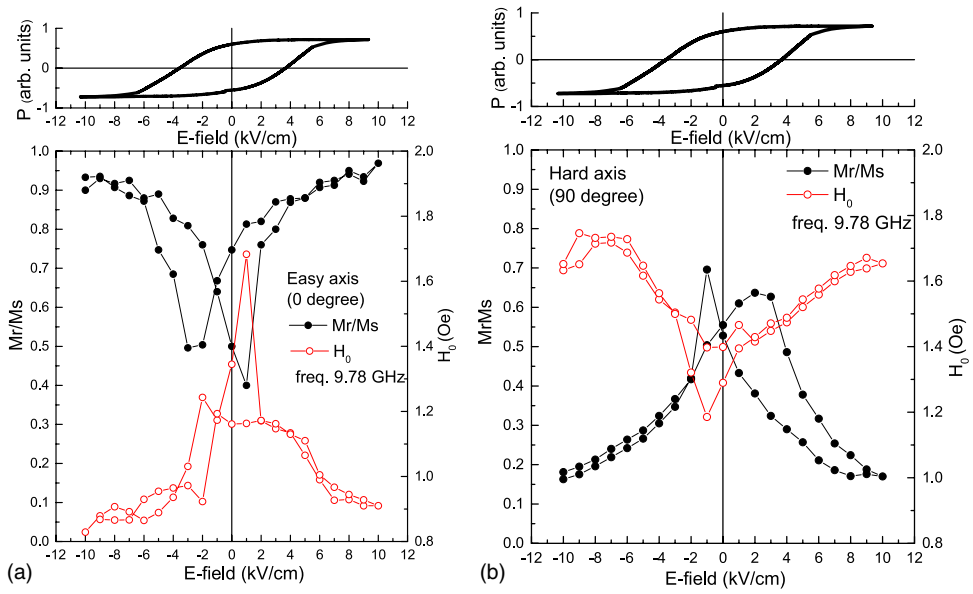

FIG. 2. PMN-PT/FePt measured along the (a) easy axis, E-field variation of squareness factor, M_r/M_S (filled dots), and resonance field, H_0 (open dots); (b) hard axis, E-field variation of squareness factor, M_r/M_S (filled dots), and resonance field, H_0 (open dots). The top inset of each plot is showing the ferroelectric PMN-PT polarization loop (P) against E-field.

graph in Fig. 2 show the ferroelectric hysteresis loop of this commercial PMN-PT slab. Sweeping the E-field from one of the electrical pole saturation state at ±10 kV/cm, toward the opposite pole saturation state at ∓10 kV/cm, it is possible to observe that the peaks of M_r/M_S are correlated in both cases with the initial flipping of the electrical dipoles in the polarization (P) curve.

The strong in-plane anisotropic contribution of the ME coupling is also evidenced in the 2D plot of the E-field, H-field variation of the FMR absorption measurements seen in Fig. 3 (easy axis) and Fig. 4 (hard axis). To conduct the FMR spectra measurements, the same protocol mentioned above for the E-field magnetic hysteresis loops was followed. In the FMR spectra, the resonance field (H_0) is defined as the field value in which the absorption derivative curve is crossing at zero. When the FMR measurements are carried out with H-field along the easy axis, a single absorption line is observed, with a peak-to-peak linewidth ΔH_{pp} = 500 Oe. Also, the FMR lines are clearly resolved at high E-fields. However, its intensity is drastically reduced at negative E-field values closer to −3 kV/cm, which is closer to the initial dropping of the polarization curve showed in the inset of Fig. 2. In spite of having observed similar trends along the hard axis orientation, the FMR spectra show broad and complex multiple absorption lines. In general, the absorption resonance profiles in this heterostructure are considerably broader than lines from the typical as-made fcc disordered FePt thin films. In the later case, as-made FePt thin films without any source of induced strain have shown single-line FMR linewidth with $\Delta H_{pp} \sim 140$ Oe.[9] Note that even after pole, the PMN-PT/FePt at relatively low E-field produces irreversible changes in the FMR spectrum with linewidth in at least a factor 3 times larger (H-field profiles in Figs. 3 and 4). In fact, this FMR linewidth broadening of the heterostructure can be explained due to the memory/ME strain texture effect after the initial pole of the as-made FePt film.

For both orientations, the E-field variations of H_0 butterfly curves are visualized in Fig. 2. Along the easy axis orientation, H_0 values are lower than in the case of the hard axis orientation (Figs. 2(a) and 2(b), respectively). In agreement with the E-field variation of the squareness factor, along the easy axis orientation, the E-field variation of H_0 is showing a minimum value at ±10 kV/cm and maximum closer to zero E-field values. Along the hard axis orientation, H_0 is showing a maximum value at ±10 kV/cm, and minimum closer to zero E-field values. Just for a guide to the eye, the E-field loop variation of H_0 is superimposed in each case of Fig. 3 (easy) and Fig. 4 (hard). For example, using the in-plane/easy-axis values of 910 Oe at 10 kV/cm and 1243 Oe at −2 kV/cm, the total

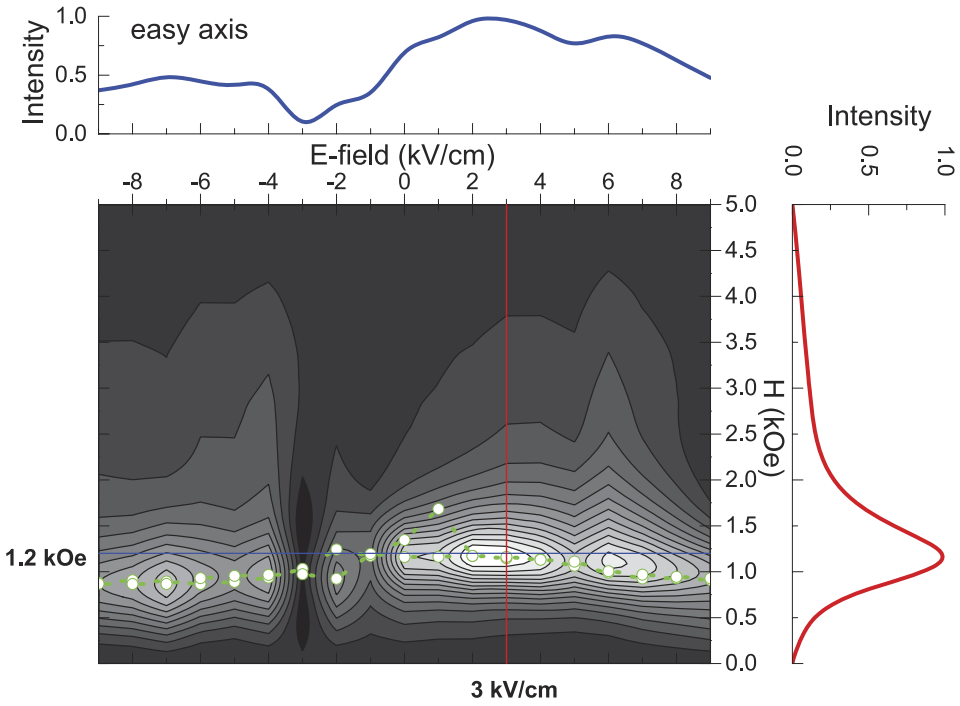

FIG. 3. PMN-PT/FePt: Easy axis orientation, 2D plot of the E-field, H-field variation of the FMR absorption measurements at X-band (9.78 GHz). The top and de side insets represent the E-field and H-field distribution profiles obtained at the location of the horizontal (blue) and vertical (red) colored lines, respectively.

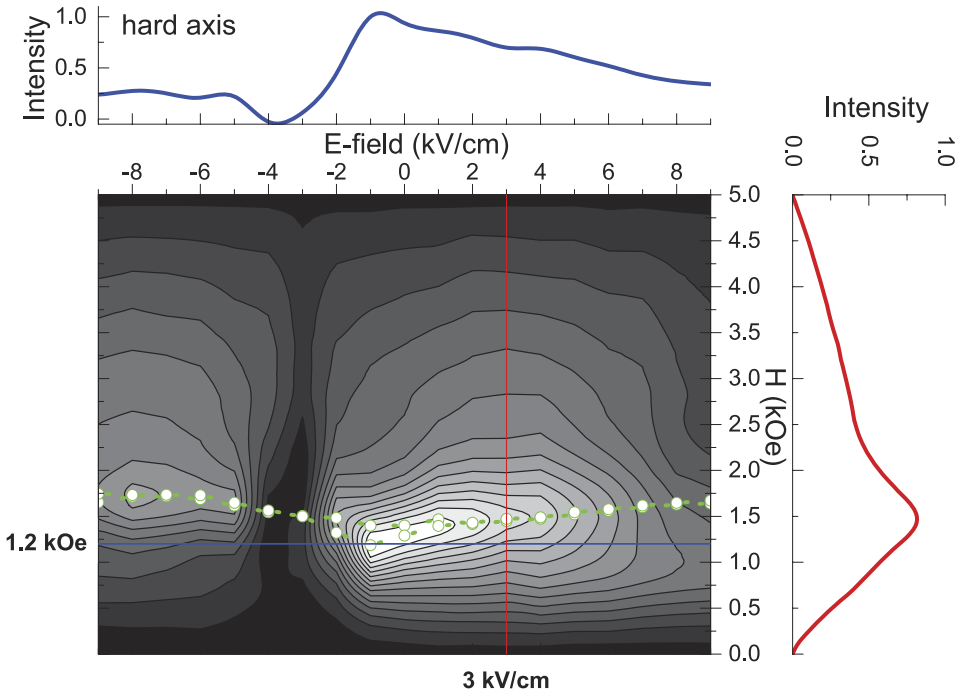

FIG. 4. PMN-PT/FePt: Hard axis orientation, 2D plot of the E-field, H-field variation of the FMR absorption measurements at X-band (9.78 GHz). The top and de side insets represent the E-field and H-field distribution profiles obtained at the location of the horizontal (blue) and vertical (red) colored lines, respectively.

resonance shift was 333 Oe, which gives a ME coefficient of 28 Oe cm kV^{-1}. In-plane/hard-axis values show a stronger ME coefficient. Using 1654 Oe at 10 kV/cm and 1185 Oe at −1 kV/cm, the total resonance shift was 469 Oe, which corresponds to a ME coefficient of 42 Oe cm kV^{-1}. In spite of this difference of ME coefficients, the easy axis FMR absorption lines are more clearly resolved lines with single and narrow shape. These ME coefficients are a factor of 3.2 and 2.2 against the respective one obtained for FeGaB/PZN-PT heterostructure, which in this case measured 94 Oe cm kV^{-1}, with an effective magnetic anisotropy field of 750 Oe and narrow FMR linewidth of 50 Oe at X-band.[13] Considering the in-plane FMR measurements along the easy and hard magnetization axes shown in Fig. 2, from the E-field variation the effective magnetic anisotropy field (H_k) can be estimated from the difference between both orientations $[H_0(hard) - H_0(easy)]_{E\text{-}field} = [2H_k]_{E\text{-}field}$.[11,16] Using this equation, a value of $H_k = 119$ Oe is obtained at 1 kV/cm and $H_k = 403$ Oe at 10 kV/cm. The detailed analysis of this fine line-shape structure is beyond the scope of this paper. Therefore, we use a simple model which provides information about the anisotropy field, H_k obtained from the magnetoelastic relations:[13] $H_k = 3\lambda_s Y d_{eff} E/M_S$, where $\lambda_s = 34 \times 10^{-6}$ (Ref. 12) is the saturation magnetostriction constant of FePt, $Y = 180$ GPa is the Young's modulus of the FePt film,[17,18] $d_{eff} = 877$ pC/N is the effective piezoelectric coefficient of the PMN-PT single crystal,[19] and E is the electric field applied to the PMN-PT single crystal. Thus, using the latter equation, the calculated values are relatively larger than the estimated ones, with values of 185 Oe at 1 kV/cm and 1859 Oe at 10 kV/cm. These values are a factor 1.5 and 4.6 larger, respectively. The difference between the estimated and calculated values of H_k can be attributed to the fact that its PMN-PT piezoelectric constant is no longer proportional to the electric field, and it is more accentuated at high electric fields.

The H_k values were also estimated from the E-field *dc* static measurements, by analyzing the relative areas between the easy/hard magnetization axis loops.[20] The following values were estimated at each E-field strength of $H_k = 110$ Oe at 1 kV/cm and $H_k = 436$ Oe at 10 kV/cm. Indeed, these values are closer to the dynamic ones, respectively. Comparing the measured and theoretical H_k values, one observes that the values obtained from X-band measurements are systematically smaller in all E-field values. A similar effect of decreasing the exchange bias values with the frequency in dynamic measurements was previously observed and explained by relaxation effects of stable and unstable magnetic grains.[21–23] Thus, E-field static and dynamic magnetization experiments allow a comprehensive understanding of the distinctive ME coupling and anisotropy field phenomena observed in this PMN-PT/FePt multiferroic heterostructure. Due to the ME coupling, it was observed that the memory/ME strain texture effect on the FePt thin film plays a key contribution in the broadening of the microwave absorption lines, larger than in the typical as-made FePt thin films with free-strain. The broadening of the FMR line suggests a major internal field dispersion in the FePt thin film which leads to an average reduction of the effective H_k values.

In summary, the static and dynamic properties of PMN-PT-FePt multiferroic heterostructure system have been studied using E-field and H-field stimuli. Each measurement method revealed facets of the ME coupling and the effective anisotropy field induced by the E-field and mediated by stress. A clear electric tuning of the microwave FMR absorption was established. To obtain E-field reliable results, we found that following the protocol mentioned here is essential. The squareness aspect ratio of the hysteresis loops provides a simple measurement of the anisotropy field and the X-band measurements allowed the investigation of the ME coupling and effective anisotropy in the dynamic regime. The dynamic response and specific form of ME tuning effect reported in this work will be used for subsequent studies to provide knowledge of the possible applications of these materials in RF and microwave tunable devices.

The authors would like to acknowledge the full support by Conicet. The authors also appreciate Dr. Alejandro Butera, Dr. Julian Milano, and Ms. Nadia Alvarez for discussions and help in sample preparation. We gratefully acknowledge contributions in manuscript preparation by Dr. Mark T. Crowley. Ferroelectric hysteresis loops were measured at the Advanced Materials Research Institute, University of New Orleans with support of Dr. Leonard Spinu. Technical support from Matias Guillén and Ruben E. Benavides is also acknowledged.

[1] A. A. Semenov, S. F. Karmanenko, V. E. Demidov, B. A. Kalinikos, G. Srinivasan, A. N. Slavin, and J. V. Mantese, Appl. Phys. Lett. **88**, 033503 (2006).
[2] G. Srinivasan, Annu. Rev. Mater. Res. **40**, 153 (2010).

[3] M. Liu, O. Obi, J. Lou, Y. Chen, Z. Cai, S. Stoute, M. Espanol, M. Lew, X. Situ, K. S. Ziemer, V. G. Harris, and N. X. Sun, Adv. Funct. Mater. **19**, 1826 (2009).
[4] G.-M. Yang, X. Xing, A. Daigle, M. Liu, O. Obi, J. W. Wang, K. Naishadham, and N. X. Sun, IEEE Trans. Magn. **44**, 3091 (2008).
[5] D. M. Pozar, *Microwave Engineering*, 4th ed. (John Wiley & Sons, Inc., November 2011).
[6] I. Stern, J. He, X. Zhou, P. Silwal, L. Miao, J. M. Vargas, L. Spinu, and D. H. Kim, Appl. Phys. Lett. **99**, 082908 (2011).
[7] T. Wu, P. Zhao, M. Bao, A. Bur, J. L. Hockel, K. Wong, K. P. Mohanchandra, C. S. Lynch, and G. P. Carman, J. Appl. Phys. **109**, 124101 (2011).
[8] K. H. Lam, C. Y. Lo, J. Y. Dai, H. L. W. Chan, and H. S. Luo, J. Appl. Phys. **109**, 024505 (2011).
[9] M. V. Mansilla, J. Gomez, E. S. Leva, F. C. Gamarra, A. A. Barahona, and A. Butera, J. Magn. Magn. Mater. **321**, 2941 (2009).
[10] E. S. Leva, R. C. Valente, F. M. Tabares, M. V. Mansilla, S. Roshdestwensky, and A. Butera, Phys. Rev. B **82**, 144410 (2010).
[11] N. Alvarez, G. Alejandro, J. Gomez, E. Goovaerts, and A. Butera, J. Phys. D: Appl. Phys. **46**, 505001 (2013).
[12] F. E. Spada, F. T. Parker, C. L. Platt, and J. K. Howard, J. Appl. Phys. **94**, 5123 (2003).
[13] J. Lou, M. Liu, D. Reed, Y. Ren, and N. X. Sun, Adv. Mater. **4711**, 21 (2009).
[14] Y. N. Zhang and R. Q. Wu, Phys. Rev. B **82**, 224415 (2010).
[15] See supplementary material at http://dx.doi.org/10.1063/1.4900815 for sample details and microstructure, Figure S1; details of magnetic images, Figure S2; and details of X-ray patterns and structural information, Figures S3 and S4, respectively.
[16] C. Vittoria, *Microwave Properties of Magnetic Films* (World Scientific, Singapore, 1993), p. 87.
[17] P. Rasmussen, X. Rui, and J. E. Shield, Appl. Phys. Lett. **86**, 191915 (2005).
[18] S. N. Hsiao, F. T. Huan, H. W. Chang, H. W. Huang, S. K. Chen, and H. Y. Lee, Appl. Phys. Lett. **94**, 232505 (2009).
[19] The piezoelectric coefficients are approximately −890 pC/N along (100) hard axis, and +290 pC/N along (01-1) easy axis, respectively (Ref. 6). The Poisson ratio, ν, of the FePt film is 0.33 (Ref. 12).
[20] N. Alvarez, E. S. Leva, R. C. Valente, M. V. Mansilla, J. Gómez, J. Milano, and A. Butera, J. Appl. Phys. **115**, 083907 (2014).
[21] J. Geshev, L. G. Pereira, J. E. Schmidt, L. Nagamine, E. B. Saitovitch, and F. Pelegrini, Phys. Rev. B **67**, 132401 (2003).
[22] N. N. Phuoc, F. Xu, Y. G. Ma, and C. K. Ong, J. Magn. Magn. Mater. **321**, 2685 (2009).
[23] S. Khanal, A. Diaconu, J. M. Vargas, D. R. Lenormand, C. Garcia, C. A. Ross, and L. Spinu, J. Phys. D:Appl. Phys. **47**, 255002 (2014).